Computer simulation of medium-range order in liquid and glassy alloys: finite-size and self-averaging effects

1996 J. Phys.: Condens. Matter 8 5269

(http://iopscience.iop.org/0953-8984/8/29/004)

J. Phys.: Condens. Matter **8** (1996) 5269–5280. Printed in the UK

Computer simulation of medium-range order in liquid and glassy alloys: finite-size and self-averaging effects

J Hafner and Ch Becker

Institut für Theoretische Physik and Centre for Computational Materials Science, Technische Universität Wien, Wiedner Hauptstraße 8-10, A-1040 Wien, Austria

Received 14 March 1996

Abstract. Detailed molecular dynamics (MD) studies of the origin of medium-range order in the liquid and glassy phases of $Ni_{81}B_{19}$ alloys are presented. Particular attention is devoted to the investigation of finite-size and self-averaging effects. It is shown that already in the liquid phase the preferred Ni–B bonding leads to the formation of B-enriched regions with the approximate stoichiometry of the crystalline Ni_3B compounds and correlation lengths of 10 to 20 Å. If the MD simulations are performed for ensembles of medium size (1000 to 1500 atoms) where the diameter of the MD cell is not much larger than the correlation length, the amplitude of the long-wavelength concentration fluctuations continues to oscillate even after very long runs ($>10^5$ steps). No such oscillations are observed in much larger ensembles (10^4 atoms). Pair correlation functions and static structure factors obtained in both simulations are in good agreement if the time averages over the smaller ensemble cover several periods of the oscillations in the concentration fluctuations. The effects of these oscillations on simulated quench experiments for the glassy phase are discussed and it is shown that good agreement with small-angle diffraction experiments can be achieved.

1. Introduction

By now, attempts to study the structure of amorphous metallic alloys have a long history. In the first stage, the debate was dominated by the homogeneously disordered versus microcrystalline controversy [1]. Soon after this was settled in favour of homogeneously disordered (i.e. truly amorphous) models, it became evident that many metallic glasses, and the transition-metal–metalloid (TM–M) glasses in particular, possess a rather strong chemical and also to a certain degree a topological short-range order. Whether the origin of this short-range order (SRO) is properly ascribed to the packing of certain stereochemical units defined in relation to the corresponding crystalline intermetallic compounds (for the TM–M glasses these would be the trigonal TM_6M prisms, the building blocks of many crystalline TM borides and phosphides) [2] or to the modulation of the dense random packing of the atoms by a preferential TM–M interaction is still the subject of discussions [3]. Recent modelling studies on the basis of realistic pair interactions [4, 5] as well as the reverse Monte Carlo analyses of the experimental data [6, 7] tend to agree that the two pictures are not entirely contradictory and that there is a continuous transition between the two regimes.

More recently, it has also become evident that many glasses also show at least some degree of medium-range order (MRO). In many TM–M [8–11] and also TM–TM [12] glasses, small-angle scattering experiments have revealed that the structure is not entirely

0953-8984/96/295269+12$19.50

homogeneous, but contains structural fluctuations, sometimes even on two different length scales [8]. Small-angle intensities in the region where $Q > 0.1$ Å^{-1} have been shown to follow a Guinier law and to indicate fluctuations with Guinier radii of the order of ten Å. The analysis of the variation of these intensities with isotopic [9] or isomorphic substitution [12] has allowed us to assign the small-angle scattering in this region to fluctuations in the concentration rather than in the density. For the Fe boride and Ni boride glasses with about 20 at.% B these concentration fluctuations have been interpreted as arising from the formation of small B-enriched regions of composition $Fe(Ni)_3B$ in a B-depleted matrix. This interpretation has been confirmed by detailed molecular dynamics studies on Fe_xB_{1-x} glasses, based on realistic interatomic forces from tight-binding-bond theory [13, 14]. In small-angle neutron scattering experiments for $Q < 0.1$ Å^{-1} a power-law behaviour of the intensities has been detected whose origin has been attributed to inner surfaces with fractal character [8]. In the present work we shall be concerned uniquely with the fluctuations characterizing the MRO.

The correct description of the MRO represents a twofold challenge to modelling studies: (i) the size of the model should be large compared to the characteristic length scale of the MRO; and (ii) if the MRO arises predominantly from concentration fluctuations, the time-scale for reaching thermodynamic equilibrium is set by the interdiffusion rate and this requires very long modelling runs. The problem became evident in two recent MD studies of the structure of TM–M glasses: while Hausleitner *et al*, using realistic interatomic interactions derived from tight-binding-bond theory [13, 14] found structures showing concentration fluctuations on a length-scale of ∼13 Å , Thijsse and Sietsma [15], using essentially the same potentials, found that the incipient phase separation is much more pronounced. The essential difference is a much longer equilibration in the liquid phase before the quench in the simulations performed by Thijsse and Sietsma, although the MD runs of Hausleitner *et al* could be considered as converged according to the usual criteria. To clarify the reasons for this apparent contradiction we present here simulations with much longer runs and on much larger ensembles allowing us to study the importance of size and self-averaging effects in MD studies of metallic glasses.

2. Molecular dynamics simulations of the liquid phase

2.1. Interatomic forces

We adopt here the effective pair and volume forces derived by Hausleitner and Hafner from hybridized nearly-free-electron–tight-binding-bond theory [4, 13]. The description of the s-electron-mediated interaction via pseudopotential and linear response theories [16] and of the covalent TM d–M p interactions via tight-binding-bond theory results in strongly non-additive pair forces with a preferential metal–metalloid interaction. The potentials for $Ni_{81}B_{19}$ are shown in figure 1. The most important aspect is the strong non-additivity of the forces: the Ni–B potential shows by far the strongest attractive interactions and the smallest diameter for the repulsive part of the potential. This is the consequence of a very strong hybridization of the B p states with the Ni d band. On the other hand, the nearly complete filling of the Ni d band leads to population of antibonding states and hence to a low bond order for the Ni–Ni bonds. The B–B forces are repulsive up to rather long distances due to a large covalent radius for the B p states (for a detailed discussion of the tight-binding-bond approach to interatomic forces in transition-metal–metalloid alloys, see [13]). From the form of the potentials it is clear that direct B–B neighbours are energetically disfavoured. Packing considerations lead to the following relation between the ratio of the Ni–B and

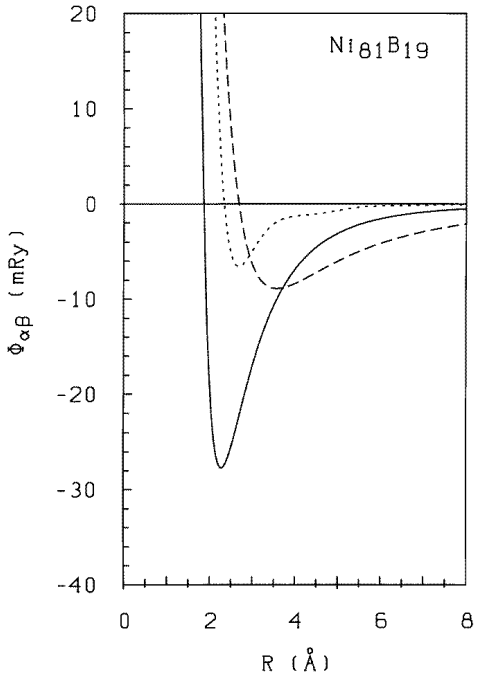

Figure 1. Interatomic pair potentials for $Ni_{81}B_{19}$ at a density of $n = 0.0967$ Å^{-3}, derived from hybridized nearly free-electron–tight-binding-bond theory. Full line: Ni–B; short dashes: Ni–Ni; long dashes: B–B potential.

Ni–Ni distances d_{Ni-B} and d_{Ni-Ni} and the average B–Ni coordination number of N_c^{B-Ni} (see [16])

$$\frac{N_c^{B-Ni}}{13} = \left(\frac{d_{Ni-B}}{d_{Ni-Ni}}\right)^3.$$

If the most probable Ni–B and Ni–Ni distances are determined by the minima in the respective potentials, we find $N_c^{B-Ni} \sim 9.6$ and this is very close to the B–Ni coordination number $N_c^{B-Ni} = 9$ in the cementite-type compound Ni_3B. Hence we can expect that the strongest tendency towards short-range order will appear at a composition of 75 at.% Ni. Using these forces, canonical MD simulations for the liquid alloy (at a density corresponding to the amorphous phase) have been performed (i) for a 'small' ensemble with $N = 1372$ atoms and (ii) for a 'large' ensemble with $N = 10\,000$ atoms.

2.2. MD simulations for the small ensemble

The simulations for the ensemble of $N = 1372$ atoms were started with Ni and B atoms distributed at random over the sites of a face-centred-cubic lattice. The lattice constant was $a = 3.458$ Å, corresponding to the density $n = 0.0967$ Å^{-3} of the metallic glass and a diameter of the MD box of 24.21 Å. The time increment was set to $\Delta t = 10^{-15}$ s. A fourth-order predictor–corrector algorithm was used for the integration of the Newtonian equations of motion [17, 18]. With this value of Δt, the total energy remains constant within four leading digits over many thousands of integration steps.

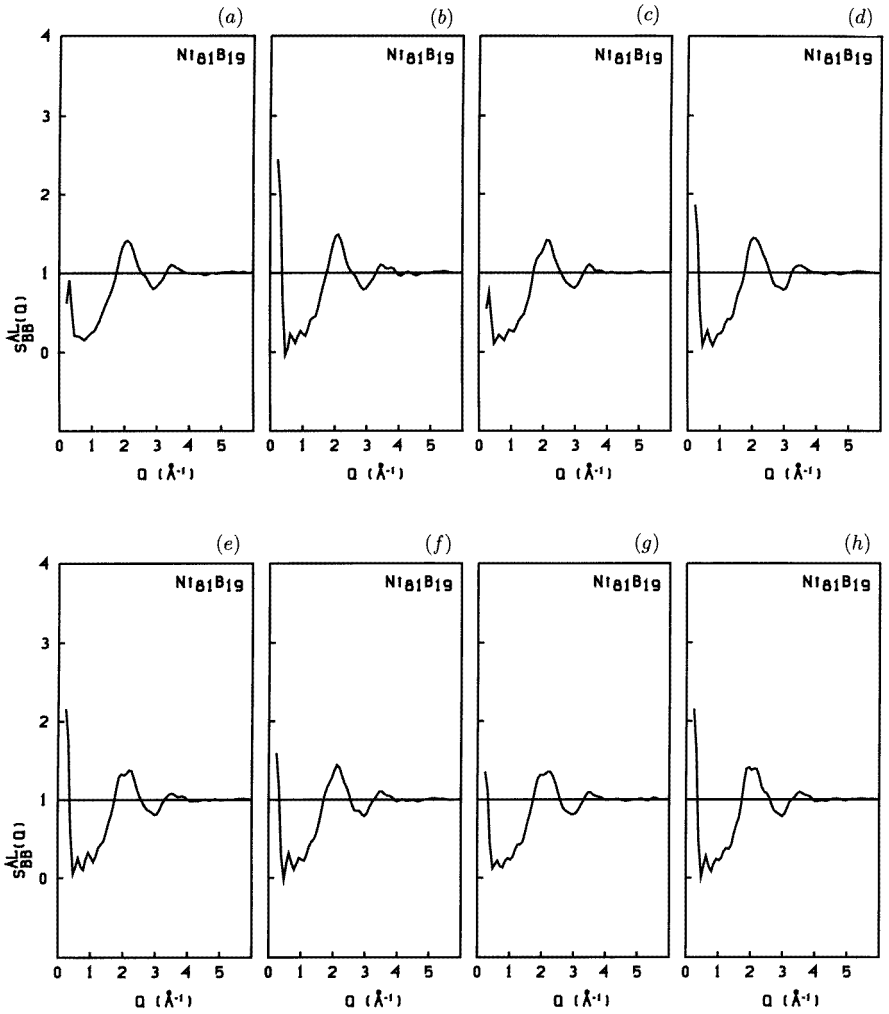

Figure 2. The partial Ashcroft–Langreth structure factor $S^{AL}_{BB}(Q)$ for boron–boron pairs in liquid $Ni_{81}B_{91}$ at $T = 2023$ K, plotted at intervals of 16 000 time steps ($=1.6\times10^{-11}$ s).

The system was first molten at a temperature of $T = 2024$ K, i.e. about 650 K above the equilibrium liquidus temperature. About 4000 to 5000 steps are necessary for melting and the initial equilibration. The evolution of the system has than been followed over a very long run of 120 000 steps, i.e. over 1.2×10^{-10} s. The most significant result is shown in figure 2: although the potential energy does not show any significant drift after the equilibration phase, the chemical medium-range order (CMRO)—as shown by the small-Q part of the B–B partial Ashcroft–Langreth structure factor $S_{BB}(Q)$—continues to increase for about 16 000 steps (note that the shortest Q-vector compatible with the periodic boundary conditions is $Q = 0.26$ Å^{-1}). The strong small-angle signal in $S_{BB}(Q)$ is indicative of an incipient phase separation in B-enriched and B-depleted regions. However, after reaching a maximum, the CMRO *decreases* again, and after 33 000 steps, the system has again reached a much more homogeneous distribution of the B atoms. Note that while the medium-range

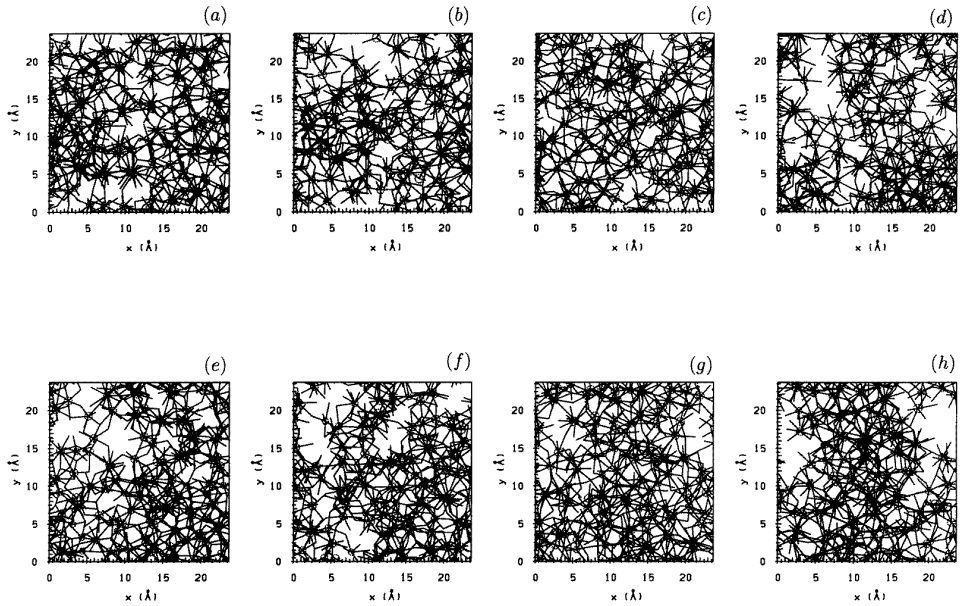

Figure 3. Projections of the instantaneous atomic positions in a slice of the 1372-atom model 5 Å thick for liquid $Ni_{81}B_{19}$ onto the xy-plane. The projections correspond to the state for which the B–B partial static structure factors are shown in figure 2. For the sake of clarity, only the B atoms (circles) and the B–Ni bonds (spokes) are shown. See the text.

order shows a strong variation, the short-range order is hardly affected at all: The position and amplitude of the first peak in $S_{BB}(Q)$ remain almost unchanged.

That the variations in the long-wavelength part of $S_{BB}(Q)$ reflect fluctuations in the local B concentrations over larger distances is also illustrated in figure 3 in the form of a projection of a slice of our model, 5 Å thick, onto the xy-plane. In this projection we show only the B atoms and the network of B–Ni bonds (at this composition there are no direct B–B neighbours [13]). One clearly sees that after 16 000 steps, distinct B-depleted regions have formed (figure 3(b)), whereas after 33 000 steps, the system has returned to the much more homogeneous initial distribution (figures 3(a) and 3(c)). The fluctuations in CSRO continue over the entire run (see figures 2 and 3).

The analysis of the complete set of reduced pair distribution functions shows that the fluctuations affect only the B–B correlations (figure 4): in a configuration showing incipient segregation (figures 2(e) and 3(e)), the reduced B–B distribution function $G_{BB}(R)$ oscillates around slowly decreasing positive values up to distances of about 10 Å and falls below zero at large R, whereas in the more homogeneous configuration reached 10 000 steps later it oscillates around zero even for the largest distances accessible in the model. The distribution functions $G_{NiB}(R)$ and $G_{NiNi}(R)$ on the other hand remain completely unaffected.

The projections of the model shown in figure 3 suggest a possible origin of this curious effect: the diameters of the B-enriched regions are of the order of 10 to 15 Å, i.e. of the same order of magnitude as the linear dimension of the MD cell (edge length 24.2 Å). The B-enriched regions are formed and destroyed in a dynamic equilibrium. If this argument is correct and if the correlation length of 10 to 15 Å corresponds to thermal equilibrium, the time dependence of the amplitude of the long-wavelength concentration fluctuations

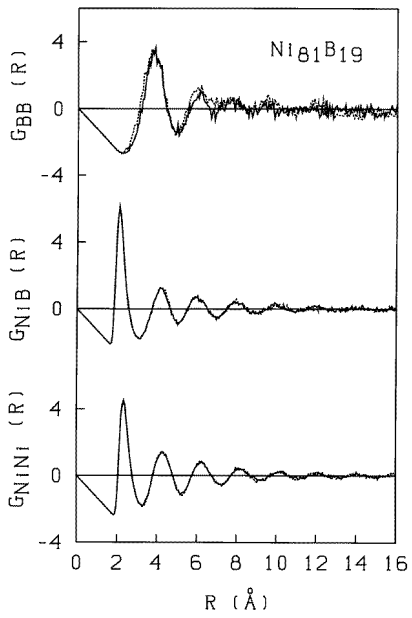

Figure 4. Partial reduced radial distribution functions $G_{BB}(R)$, $G_{NiB}(R)$ and $G_{NiNi}(R)$ for liquid $Ni_{81}B_{19}$. The full lines show the distribution functions for a more homogeneous configuration (corresponding to part (*g*) in figures 2 and 3), while the broken lines show that for a configuration where the tendency to segregation in B-rich and B-depleted regions is more pronounced (cf. part (*e*) in figures 2 and 3).

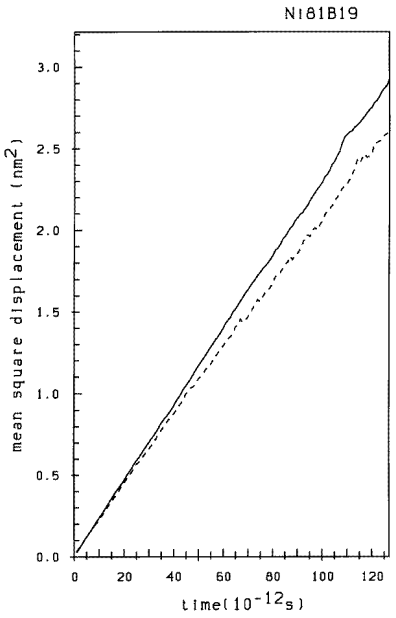

Figure 5. Mean square displacements of Ni (full lines) and B (broken lines) atom in liquid $Ni_{81}B_{19}$.

should disappear in a larger ensemble, where the ensemble average itself corresponds to an extended time average over the smaller ensemble. The problem is whether the extension to a larger ensemble eventually also leads to significant modifications in the correlations functions outside the small-angle region, i.e. whether the smaller ensemble shows finite-size effects that do not disappear after an extended ensemble average.

Before describing the results obtained with a much larger ensemble, we briefly mention the results obtained for the diffusion coefficients. Figure 5 shows the mean square displacements of Ni and B atoms, calculated over this very extended MD run. From the slope of the curves, we obtain diffusion coefficients of $D_{Ni} = 2.3 \times 10^{-9}$ m^2 s^{-1} and $D_B = 2.0 \times 10^{-9}$ m^2 s^{-1}, respectively. If just the nominal atomic sizes are considered, the result that the Ni atoms diffuse faster than the B atoms might appear to be counterintuitive. However, we have to remember that the B–B nearest-neighbour interactions are repulsive, and that there are very strong Ni–B interactions confining the B atoms within the cage of the surrounding Ni atoms.

2.3. MD simulations for the large ensemble

To check this point, the MD simulations have been repeated for a much larger ensemble of $N = 10\,000$ atoms. In this model the linear dimension of the MD cell is 46.93 Å, corresponding to a shortest wavevector of $Q = 0.13$ Å^{-1}. All other parameters of the

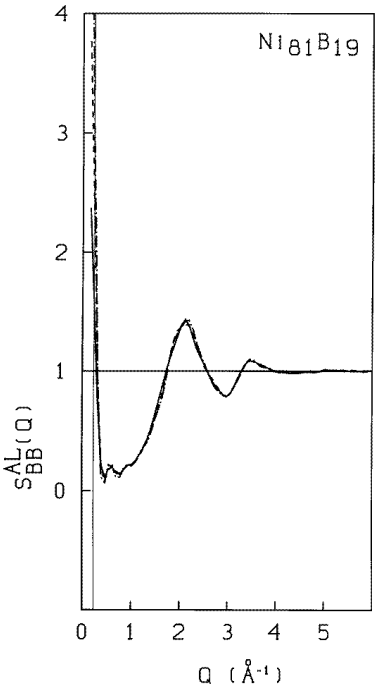

Figure 6. The partial Ashcroft–Langreth structure factor $S^{AL}_{BB}(Q)$ for a B–B pair calculated for the 10 000-atom ensemble after 1, 2, and 3×10^4 time steps (full, dashed and dot–dashed lines). The thin vertical line indicates the smallest wavenumber compatible with the periodic boundary conditions for the smaller 1372-atom ensemble. See the text.

simulation are unchanged; the run has been extended over about 30 000 time steps.

Figure 6 shows again the B–B partial structure factors calculated after 1, 2, and 3×10^4 time steps. Although initially there is a slow increase of $S_{BB}(Q)$ for the smallest wavevectors, there are no indications for a time dependence of the long-range concentration fluctuations. The same picture also results from a direct inspection of the three-dimensional structure: the projections shown in figure 7 demonstrate that there are indeed structural inhomogeneities in the system in the form of B-enriched and B-depleted regions. The characteristic distance between these regions can be estimated to be 15 to 20 Å, i.e., only slightly larger than the simulations on the smaller systems had suggested. This would confirm that the correct ensemble average, which is obtained for the small system only after an extended time average, is obtained for the large system after much shorter runs, due to the self-averaging properties of the larger ensemble.

For the structural properties, both sets of simulations lead to completely equivalent results. This is demonstrated in figure 8: for the Ni–Ni and Ni–B correlations the two sets of partial structure factors and reduced radial distribution functions are identical. For the B–B structure factor we note a minimal difference in the small-Q regime. In the B–B distribution function we find a slightly larger diameter of the B-enriched regions in the simulations with the large ensemble compared to those with the smaller ensemble, as already discussed above. Altogether, the comparison of the results obtained with the large and small ensembles confirms our expectation: the time-dependent medium-range concentration fluctuations disappear in the averages taken over the large ensemble because the system

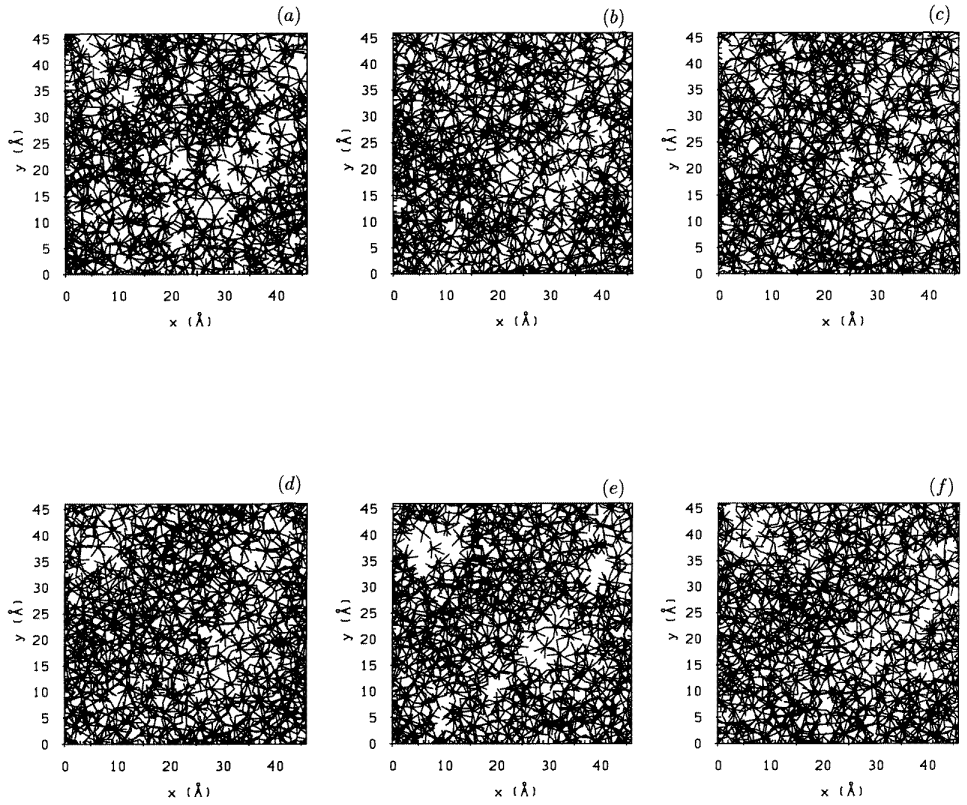

Figure 7. Projections of a slice of the 10 000-atom model onto the xy-plane. Instantaneous configurations after about 0.5, 1, 1.5, 2, 2.5 and 3×10^4 time steps are shown. Compare figure 6 and the text.

size is large enough for self-averaging to occur even for fluctuations with a rather large correlation length.

3. The simulated quench experiment

Finally, we want to briefly address the problem of the simulation of the glassy phase, and the dependence of the results of the simulated quench on the concentration-fluctuation effects discussed above. Evidently the results obtained with the small ensemble will depend to some degree on the state of the liquid system in the moment at which the quench starts. We investigate this for two states showing strong and weak segregation effects. In both cases the quenching rate is about 10^{12} K s^{-1}, and the cooling run starts at $T = 2023$ K and continues until room temperature is reached. The volume is constant during the quench. If we start from a liquid configuration showing strong demixing effects (configuration (b) in figure 2), the B–B partial structure factor indicates a weak enhancement of both the SRO (as measured by the amplitude of the main peak = prepeak in $S_{BB}(Q)$ and in the concentration-fluctuation structure factor $S_{CC}(Q)$) and in the MRO (as measured by the small-angle amplitude); see figure 9. If we start from a more homogeneous configuration (state (c) in figure 2), we find a continuous increase of the SRO during the quench, but the

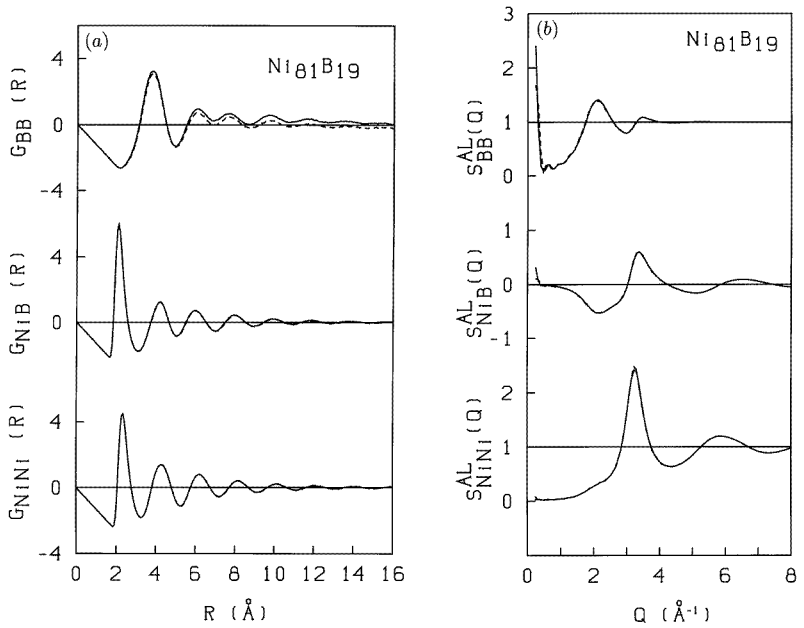

Figure 8. Partial reduced radial distribution functions $G_{ij}(R)$, $i, j =$ Ni, B (a) and Ashcroft–Langreth partial static structure factors $S_{ij}^{AL}(Q)$ (b) for $Ni_{81}B_{19}$. Full lines: a large ensemble (10 000 atoms) and 3×10^4 time steps; broken lines: a small ensemble (1372 atoms) and 12×10^4 time steps.

MRO increases slightly only during the final annealing stages for the glassy sample at room temperature. Altogether, the small-angle peak remains much weaker than for the first run. The other partial structure factors are essentially identical to those obtained in our previous MD study of Ni–B glasses [13].

It turns out to be very difficult to establish a clear trend for changes in the SRO that are possibly induced by the differences in the MRO: if the quench is started from the more homogeneous liquid configuration, the first peak in $S_{BB}(Q)$ is relatively asymmetric (with a shoulder on the left-hand side) before the quench, but quite symmetric in the glassy state (figure 9(b)). If the quench proceeds from a configuration with stronger medium-range concentration fluctuations, the main peak in $S_{BB}(Q)$ is almost symmetric in the liquid phase, but assumes an asymmetric form with a left-hand shoulder in the glassy state. This result indicates, in agreement with the conclusions drawn from the results for the liquid alloys, that the fluctuations observed in the MRO and SRO are only weakly coupled. In any case, if relatively small MD ensembles are used to investigate MRO and SRO effects in glassy alloys, an average must be taken over a representative set of different starting configurations, which is similar to the 'inherent structure approach' proposed by Stillinger and Weber [19] and used by one of the present authors for a series of metallic glasses [20]. No such dependence on the starting state is expected nor observed in simulations with the large ensemble where the resulting $S_{BB}(Q)$ for the glassy alloy is essentially identical with the average over the results shown in parts (a) and (b) of figure 9. For a detailed comparison with the large-angle diffraction data, we refer again to our previously published results [13]. Except for the small-angle region and the small changes in the prepeak of $S_{BB}(Q)$ arising from an average over different quenched configurations, these results remain perfectly valid.

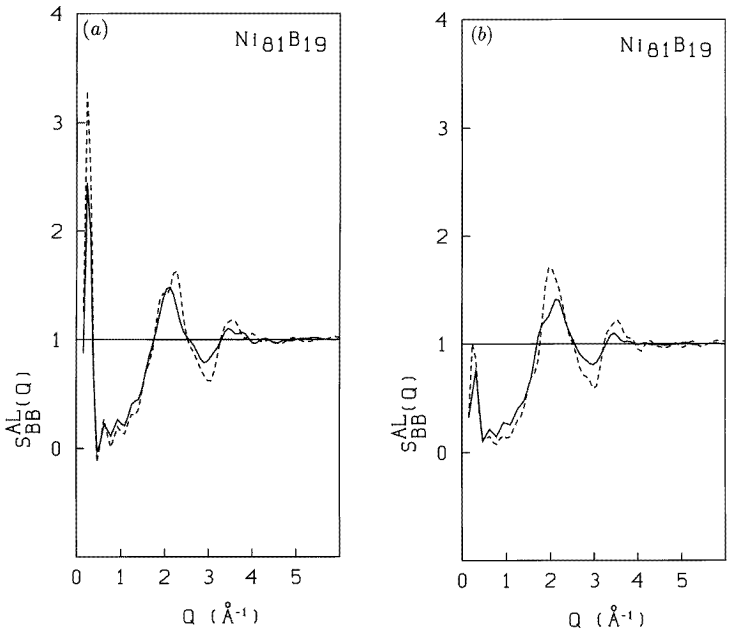

Figure 9. The B–B static structure factor of glassy $Ni_{81}B_{19}$, produced by a quench starting from a liquid state with a strong demixing tendency (*a*) and from a state with a more homogeneous distribution of the B atoms (*b*). See the text.

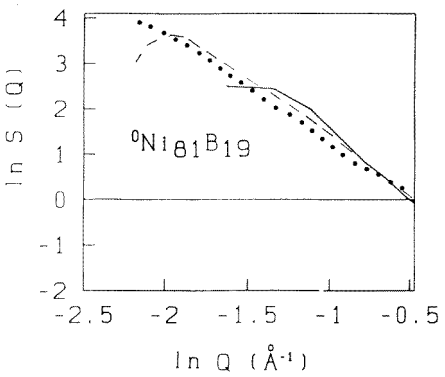

Figure 10. The neutron-weighted total static structure factor $S(Q)$ ($\propto S_{BB}(Q)$) for amorphous $^0Ni_{81}B_{19}$ prepared with an isotope mixture for Ni having zero average scattering length. Full line: an MD simulation for a 1372-atom ensemble (configuration average); dashed line: MD results for the 10 000-atom ensemble; full dots: small-angle neutron scattering [8].

In the small-angle region we can compare the simulation results with small-angle neutron scattering experiments on isotope-substituted $Ni_{81}B_{19}$ glasses [8]. If the glassy alloy is prepared with a mixture of Ni isotopes having zero average scattering length, the scattering intensity is determined by the B–B partial structure factor alone. Figure 10 compares the experimental results with the small-angle intensities calculated for a large ensemble and for an average over quenched configurations of the smaller ensemble. Differences between the two ensembles appear only at wavenumbers lower than the limit imposed by

the periodic boundary conditions of the smaller ensemble. Beyond this limit, the good agreement between the two theoretical results confirms the self-averaging properties of the large ensemble; the agreement between theory and computer simulation confirms that the MRO is indeed dominated by concentration fluctuations. This is also in accordance with our results on the MRO in Fe–B glasses [14].

4. Conclusions

We have analysed the description of medium-range-order effects (and of medium-range concentration fluctuations in particular) in liquid and amorphous materials via molecular dynamics simulations. We have shown that the interplay of a strong preference for heterocoordination and of packing effects can induce medium-range dynamical concentration fluctuations in the liquid phase. If the diameter of the MD ensemble is only about twice the correlation length of the concentration fluctuations, their amplitude continues to oscillate even over very long runs. Only simulations on much larger ensembles reach a stable equilibrium with respect to medium-range fluctuations. Long-time averages over the smaller ensembles are in good agreement with the results obtained in relatively short runs on the larger ensembles, indicating the self-averaging properties of the large ensembles.

Our results explain the origin of the discrepancies observed between earlier simulations [13, 15] on smaller ensembles. These results were reasonably well converged as far as the SRO is concerned, but not with respect to the MRO. The quench from the liquid phase was started from configurations with distinctly different amplitudes of the medium-range concentration fluctuations.

Together with our previous studies of MRO in Fe–B glasses (based again on simulations for a 10 000-atom ensemble) [14], the present work shows that medium-range concentration fluctuations are a common feature of amorphous transition-metal–metalloid alloys and that they are well described in MD simulations on the basis of tight-binding-bond potentials, provided that these simulations are based on sufficiently large ensembles and/or very extended time averages.

Acknowledgments

This work has been supported by the Austrian Ministery for Science, Research and Art through the Centre for Computational Materials Science (CMS).

References

[1] Cargill G S 1975 *Solid State Physics, Advances in Research and Applications* vol 30, ed F Seitz and D Turnbull (New York: Academic) p 227
[2] Gaskell P H 1983 *Glassy Metals II* ed H Beck and H J Güntherodt (Berlin: Springer) p 5
[3] Lamparter P and Steeb S 1993 Structure of amorphous and molten materials *Materials Science and Technology* vol 1, ed R W Cahn and P Haasen (Weinheim: Chemie) p 217
[4] Hausleitner C and Hafner J 1992 *Phys. Rev.* B **45** 128
[5] Kreuch G and Hafner J 1995 *J. Non-Cryst. Solids* **189** 227
[6] Lamparter P 1995 *Phys. Scr.* T **57** 45
[7] Iparraguire E W, Sietsma J, Thijsse B J and Pusztai L 1993 *Comput. Mater. Sci.* **1** 110
[8] Lamparter P and Steeb S 1988 *J. Non-Cryst. Solids* **106** 137
[9] Schild K, Frisius F, Lamparter P and Steeb S 1985 *Z. Naturf.* a **40** 551
[10] Faigel S and Svab E 1985 *Rapidly Quenched Metals V* ed S Steeb and H Warlimont (Amsterdam: North-Holland) p 487

[11] Yavari A R 1985 *Rapidly Quenched Metals V* ed S Steeb and H Warlimont (Amsterdam: North-Holland) p 495
[12] Maret M, Simon J P and Lyon O 1989 *J. Phys.: Condens. Matter* **1** 10 249
[13] Hausleitner C and Hafner J 1993 *Phys. Rev.* B **47** 5689
[14] Hausleitner C, Hafner J and Becker C 1993 *Phys. Rev*. B **48** 13 119
[15] Thijsse B J and Sietsma J 1994 *Mater. Sci. Eng.* A **179+178** 438
[16] Heine V and Weaire D 1970 *Solid State Physics* vol 24, ed H Ehrenreich and D Turnbull (New York: Academic) p 424
[17] Arnold A, Mauser N and Hafner J 1989 *J. Phys.: Condens. Matter* **1** 965
[18] Gear C W 1966 *Numerical Initial Value Problems in Ordinary Differential Equations* (Englewood Cliffs, NJ: Prentice-Hall) chs 9, 10
[19] Stillinger F H and Weber T A 1984 *J. Chem. Phys.* **80** 4434
[20] Hafner J 1988 *J. Phys. F: Met. Phys.* **18** 153